Z. Phys. C - Particles and Fields 53, 567-580 (1992)

Zeitschrift für Physik C Particles and Fields

Measurement of the average lifetime of *B* hadrons

DELPHI Collaboration

P. Abreu[18], W. Adam[43], F. Adami[34], T. Adye[32], T. Akesson[21], G.D. Alekseev[13], P. Allen[42], S. Almehed[21], S.J. Alvsvaag[4], U. Amaldi[7], E. Anassontzis[3], P. Antilogus[22], W-D. Apel[14], R.J. Apsimon[32], B. Åsman[38], P. Astier[20], J-E. Augustin[16], A. Augustinus[27], P. Baillon[7], P. Bambade[16], F. Barao[18], R. Barate[11], G. Barbiellini[40], D.Y. Bardin[13], A. Baroncelli[35], O. Barring[21], W. Bartl[43], M.J. Bates[30], M. Battaglia[25], M. Baubillier[20], K-H. Becks[45], C.J. Beeston[30], M. Begalli[10], P. Beilliere[6], Yu. Belokopytov[37], P. Beltran[9], D. Benedic[8], J.M. Benlloch[42], M. Berggren[38], D. Bertrand[2], F. Bianchi[39], M.S. Bilenky[13], P. Billoir[20], J. Bjarne[21], D. Bloch[8], S. Blyth[30], V. Bocci[33], P.N. Bogolubov[13], T. Bolognese[34], M. Bonapart[27], M. Bonesini[25], W. Bonivento[25], P.S.L. Booth[19], M. Boratav[20], P. Borgeaud[34], G. Borisov[37], H. Borner[7], C. Bosio[35], B. Bostjancic[7], O. Botner[41], B. Bouquet[16], M. Bozzo[10], S. Braibant[2], P. Branchini[35], K.D. Brand[31], R.A. Brenner[12], C. Bricman[2], R.C.A. Brown[7], N. Brummer[27], J-M. Brunet[6], L. Bugge[29], T. Buran[29], H. Burmeister[7], J.A.M.A. Buytaert[7], M. Caccia[7], M. Calvi[25], A.J. Camacho Rozas[36], A. Campion[19], T. Camporesi[7], V. Canale[33], F. Cao[2], F. Carena[7], L. CArroll[19], C. Caso[10], E. Castelli[40], M.V. Castillo Gimenez[42], A. Cattai[7], F.R. Cavallo[5], L. Cerrito[33], A. Chan[1], P. Charpentier[7], P. Checchia[31], G.A. Chelkov[13], L. Chevalier[34], M. Chiapkin[37], P. Chliapnikov[37], V. Chorowicz[20], R. Cirio[39], M.P. Clara[39], P. Collins[30], J.L. Contreras[23], R. Contri[10], G. Cosme[16], F. Couchot[16], H.B. Crawley[1], D. Crennell[32], G. Crosetti[10], M. Crozon[6], J. Cuevas Maestro[36], S. Czellar[12], S. Dagoret[16], E. Dahl-Jensen[26], B. Dalmagne[16], M. Dam[4], G. Damgaard[26], G. Darbo[10], E. Daubie[2], P.D. Dauncey[30], M. Davenport[7], P. David[20], A. De Angelis[40], M. De Beer[34], H. De Boeck[2], W. De Boer[14], C. De Clercq[2], M.D.M. De Fez Laso[42], N. De Groot[27], C. De La Vaissiere[20], B. De Lotto[40], A. De Min[25], C. Defoix[6], D. Delikaris[7], S. Delorme[7], P. Delpierre[6], N. Demaria[39], L. Di Ciaccio[33], H. Dijkstra[7], F. Djama[8], J. Dolbeau[6], O. Doll[45], M. Donszelmann[27], K. Doroba[44], M. Dracos[7], J. Drees[45], M. Dris[28], Y. Dufour[6], W. Dulinski[8], L-O. Eek[41], P.A.-M. Eerola[7], T. Ekelof[41], G. Ekspong[38], A. Elliot Peisert[31], J-P. Engel[8], D. Fassouliotis[28], M. Feindt[7], A. Fenyuk[37], M. Fernandez Alonso[36], A. Ferrer[42], T.A. Filippas[28], A. Firestone[1], H. Foeth[7], E. Fokitis[28], P. Folegati[40], F. Fontanelli[10], K.A.J. Forbes[19], H. Forsbach[45], B. Franek[32], P. Frenkiel[6], D.C. Fries[14], A.G. Frodesen[4], R. Fruhwirth[43], F. Fulda-Quenzer[16], K. Furnival[19], H. Furstenau[14], J. Fuster[7], G. Galeazzi[31], D. Gamba[39], C. Garcia[42], J. Garcia[36], C. Gaspar[7], U. Gasparini[31], P. Gavillet[7], E.N. Gazis[28], J-P. Gerber[8], P. Giacomelli[7], K-W. Glitza[45], R. Gokieli[7], V.M. Golovatyuk[13], J.J. Gomez Y Cadenas[7], A. Goobar[38], G. Gopal[32], M. Gorski[44], V. Cracco[10], A. Grant[7], F. Grard[2], E. Graziani[35], M-H. Gros[16], G. Grosdidier[16], E. Gross[7], B. Grossetete[20], P. Grosse-Wiesmann[7], J. Guy[32], F. Hahn[7], M. Hahn[14], S. Haider[27], Z. Hajduk[27], A. Hakansson[21], A. Hallgren[41], K. Hamacher[45], G. Hamel De Monchenault[34], F.J. Harris[30], B.W. Heck[7], T. Henkes[7], I. Herbst[45], J.J. Hernandez[42], P. Herquet[2], H. Herr[7], I. Hietanen[12], C.O. Higgins[19], E. Higon[42], H.J. Hilke[7], S.D. Hodgson[30], T. Hofmokl[44], R. Holmes[1], S-O. Holmgren[38], D. Holthuizen[27], P.F. Honore[6], J.E. Hooper[26], M. Houlden[19], J. Hrubec[43], P.O. Hulth[38], K. Hultqvist[38], D. Husson[8], P. Ioannou[3], D. Isenhower[7], P-S. Iversen[4], J.N. Jackson[19], P. Jalocha[15], G. Jarlskog[21], P. Jarry[34], B. Jean-Marie[16], E.K. Johansson[38], D. Johnson[19], M. Jonker[7], L. Jonsson[21], P. Juillot[8], G. Kalkanis[3], G. Kalmus[32], F. Kapusta[20], S. Katsanevas[3], E.C. Katsoufis[28], R. Keranen[12], J. Kesteman[2], B.A. Khomenko[13], N.N. Khovanski[13], B. King[19], N.J. Kjaer[7], H. Klein[7], W. Klempt[7], A. Klovning[4], P. Kluit[27], A. Koch-Mehrin[45], J.H. Koehne[14], B. Koene[27], P. Kokkinias[9], M. Kopf[14], M. Koratzinos[39], K. Korcyl[15], A.V. Korytov[13], V. Kostukhin[37], C. Kourkoumelis[3], T. Kreuzberger[43], J. Krolikowski[44], I. Kronkvist[21], J. Krstic[30], U. Kruener-Marquis[45], W.Krupinski[15], W. Kucewicz[25], K. Kurvinen[12], C. Lacasta[42], C. Lambropoulos[9], J.W. Lamsa[1], L. Lanceri[40], V. Lapin[37], J-P. Laugier[34], R. Lauhakangas[12], G. Leder[43], F. Ledroit[11], R. Leitner[7], Y. Lemoigne[34], J. Lemonne[2], G. Lenzen[45], V. Lepeltier[16], A. Letessier-Selvon[20], D. Liko[43], E. Lieb[45], E. Lillethun[4], J. Lindgren[12], A. Lipniacka[44], I. Lippi[31], R. Llosa[23], B. Loerstad[21], M. Lokajicek[13], J.G. Loken[30], M.A. Lopez Aguera[36], A. Lopez-Fernandez[16], M. Los[27], D. Loukas[9], A. Lounis[8], J.J. Lozano[42], R. Lucock[32], P. Lutz[6], L. Lyons[30], G. Maehlum[7], N. Magnussen[45], J. Maillard[6], A. Maltezos[9], F. Mandl[43], J. Marco[36], M. Margoni[31], J-C. Marin[7], A. Markou[9], S. Marti[42], L. Mathis[6], F. Matorras[36], C. Matteuzzi[25], G. Matthiae[33], M. Matveev[37], M. Mazzucato[31], M. McCubbin[19], R. McKay[1], R. McNulty[19], E. Menichetti[39], C. Meroni[25], W.T. Meyer[1], M. Michelotto[31], W.A. Mitaroff[43], G.V. Mitselmakher[13], U. Mjoernmark[21], T. Moa[38], R. Moeller[26], K. Moenig[7], M.R. Monge[10], P. Morettini[10], H. Mueller[14], W.J. Murray[32], G. Myatt[30], F. Naraghi[20], U. Nau-Korzen[45], F.L. Navarria[5], P. Negri[25], B.S. Nielsen[26], B. Nijjhar[19], V. Nikolaenko[37], V. Obraztsov[37], A.G. Olshevski[13], R. Orava[12], A. Ostankov[37], A. Ouraou[34], M. Paganoni[25], R. Pain[20], H. Palka[27], T. Papadopoulou[28], L. Pape[7], A. Passeri[35], M. Pegoraro[31], V. Perevozchikov[37], M. Pernicka[43], A. Perrotta[5], F. Pierre[34], M. Pimenta[18], O. Pingot[2], M.E. Pol[7], G. Polok[15], P. Poropat[40], P. Privitera[14], A. Pullia[25], J. Pyyhtia[12], D. Radojicic[30], S. Ragazzi[25], P.N. Ratoff[17], A.L. Read[29], N.G. Redaelli[25], M. Regler[43], D. Reid[19], P.B. Renton[30], L.K. Resvanis[3], F. Richard[16], M. Richardson[19], J. Ridky[13], G. Rinaudo[39], I. Roditi[7], A. Romero[39], I. Roncagliolo[10], P. Ronchese[31], C. Ronnqvist[12],

E.I. Rosenberg[1], U. Rossi[5], E. Rosso[7], P. Roudeau[16], T. Rovelli[5], W. Ruckstuhl[27], V. Ruhlmann[34], A. Ruiz[36], K. Rybicki[15], H. Saarikko[12], Y. Sacquin[34], G. Sajot[11], J. Salt[42], E. Sanchez[42], J. Sanchez[23], M. Sannino[10], M. Schaeffer[8], S. Schael[14], H. Schneider[14], M.A.E. Schyns[7], F. Scuri[40], A.M. Segar[30], R. Sekulin[32], M. Sessa[40], G. Sette[10], R. Seufert[14], R.C. Shellard[7], P. Siegrist[34], S. Simonetti[10], F. Simonetto[31], A.N. Sissakian[13], T.B. Skaali[29], G. Skjevling[29], G. Smadja[34, 22], N. Smirnov[37], G.R. Smith[32], R. Sosnowski[44], T.S. Spassoff[11], E. Spiriti[35], S. Squarcia[10], H. Staeck[45], C. Stanescu[35], G. Stavropoulos[9], F. Stichelbaut[2], A. Stocchi[16], J. Strauss[45], R. Strub[8], M. Szczekowski[44], M. Szeptycka[44], P. Szymanski[44], T. Tabarelli[25], S. Tavernier[2], G. Theodosiou[9], A. Tilquin[24], J. Timmermans[27], V.G. Timofeev[13], L.G. Tkatchev[13], T. Todorov[13], D.Z. Toet[27], E. Torassa[39], L. Tortora[35], M.T. Trainor[30], D. Treille[7], U. Trevisan[10], W. Trischuk[7], G. Tristram[6], C. Troncon[25], A. Tsirou[7], E.N. Tsyganov[13], M. Turala[15], R. Turchetta[8], M-L. Turluer[34], T. Tuuva[12], I.A. Tyapkin[13], M. Tyndel[32], S. Tzamarias[7], B. Ueberschaer[45], S. Ueberschaer[45], O. Ullaland[7], V.A. Urarov[37], G. Valenti[5], E. Vallazza[39], J.A. Valls Ferrer[42], G.W. Van Apeldoorn[27], P. Van Dam[27], W.K. Van Doninck[2], C. Vander Velde[2], J. Varela[18], P. Vaz[7], G. Vegni[25], L. Ventura[31], W. Venus[32], F. Verbeure[2], L.S. Vertogradov[13], L. Vibert[20], D. Vilanova[34], L. Vitale[40], E.V. Vlasov[37], S. Vlassopoulos[28], A.S. Vodopyanov[13], M. Vollmer[45], S. Volponi[5], G. Voulgaris[3], M. Voutilainen[12], V. Vrba[35], H. Wahlen[45], C.Walck[38], F. Waldner[40], M. Wayne[1], P. Weilhammer[7], J. Werner[45], A.M. Wetherell[7], J.H. Wickens[2], J. Wikne[29], G.R. Wilkinson[30], W.S.C. Williams[30], M. Winter[8], D. Wormald[29], G. Wormser[16], K. Woschnagg[41], N. Yamdagni[38], P. Yepes[7], A. Zaitsev[37], A. Zalewska[15], P. Zalewski[44], D. Zavrtanik[7], E. Zevgolatakos[9], G. Zhang[45], N.I. Zimin[13], M. Zito[34], R. Zitoun[20], R. Zukanovich Funchal[6], G. Zumerli[31], J. Zuniga[42]

[1] Ames Laboratory and Department of Physics, Iowa State University, Ames IA-50011, USA
[2] Physics Department, Univ. Instelling Antwerpen, Universiteitsplein 1, B-2610 Wilrijk, Belgium, and IIHE, ULB-VUB, Pleinlaan 2, 1050 Brussels, Belgium, and Service de Phys. des Part. Elém., Faculté des Sciences, Université de l'Etat Mons, Av. Maistriau 19, 7000 Mons, Belgium
[3] Physics Laboratory, University of Athens, Solonos Str. 104, 10680 Athens, Greece
[4] Department of Physics, University of Bergen, Alleégaten 55, 5007 Bergen, Norway
[5] Dipartimento di Fisica, Università di Bologna and INFN, Via Irnerio 46, 40126 Bologna, Italy
[6] Collège de France, Lab. de Physique Corpusculaire, 11 pl. M. Berthelot, 75231 Paris Cedex 05, France
[7] CERN, 1211 Geneva 23, Switzerland
[8] Division des Hautes Energies, CRN - Groupe DELPHI and LEPSI, B.P. 20 CRO, 67037 Strasbourg Cedex, France
[9] Institute of Nuclear Physics, N.R.C. Demokritos, P.O. Box 60628, 15310 Athens, Greece
[10] Dipartimento di Fisica, Università di Genova and INFN, Via Dodecaneso 33, 16146 Genova, Italy
[11] Institut des Sciences Nucléaires, Université de Grenoble 1, 38026 Grenoble, France
[12] Research Institute for High Energy Physics, University of Helsinki, Siltavuorenpenger 20 C, 00170 Helsinki 17, Finland
[13] Joint Institute for Nuclear Research, Dubna, Head Post Office, P.O. Box 79, SU-101 000 Moscow, USSR
[14] Institut für Experimentelle Kernphysik, Universität Karlsruhe, Postfach 6980, W-7500 Karlsruhe 1, Federal Republic of Germany
[15] High Energy Physics Laboratory, Institute of Nuclear Physics, Ul. Kawiory 26a, PL-30055 Krakow 30, Poland
[16] Université de Paris-Sud, Lab. de l'Accélérateur Linéaire, Bat 200, 91405 Orsay, France
[17] School of Physics and Materials, University of Lancaster, Lancaster LA1 4YB, UK
[18] LIP, Av. Elias Garcia 14 - 1e, 1000 Lisbon Codex, Portugal
[19] Department of Physics, University of Liverpool, P.O. Box 147, Liverpool L69 3BX, UK
[20] LPNHE, Universités Paris VI et VII, Tour 33 (RdC), 4 place Jussieu, 75230 Paris Cedex 05, France
[21] Department of Physics, University of Lund, Sölvegatan 14, 22363 Lund, Sweden
[22] Université Claude Bernard de Lyon, 43 Bd du 11 Novembre 1918, 69622 Villeurbanne Cedex, France
[23] Universidad Complutense, Avda. Complutense s/n, 28040 Madrid, Spain
[24] Univ. d'Aix - Marseille II - Case 907 - 70, route Léon Lachamp, 13288 Marseille Cedex 09, France
[25] Dipartimento di Fisica, Università di Milano and INFN, Via Celoria 16, 20133 Milan, Italy
[26] Niels Bohr Institute, Blegdamsvej 17, 2100 Copenhagen 0, Denmark
[27] NIKHEF-H, Postbus 41882, 1009 DB Amsterdam, The Netherlands
[28] National Technical University, Physics Department, Zografou Campus, 15773 Athens, Greece
[29] Physics Department, University of Oslo, Blindern, 1000 Oslo 3, Norway
[30] Nuclear Physics Laboratory, University of Oxford, Keble Road, Oxford OX1 3RH, UK
[31] Dipartimento di Fisica, Università di Padova and INFN, Via Marzolo 8, 35131 Padua, Italy
[32] Rutherford Appleton Laboratory, Chilton, Didcot OX11 OQX, UK
[33] Dipartimento di Fisica, Università di Roma II and INFN, Tor Vergata, 00173 Rome, Italy
[34] CEN-Saclay, DPhPE, 91191 Gif-sur-Yvette Cedex, France
[35] Istituto Superiore di Sanità (INFN), Viale Regina Elena 299, 00161 Rome, Italy
[36] Facultad de Ciencias, Universidad de Santander, av. de los Castros, 39005 Santander, Spain
[37] Inst. for High Energy Physics, Serpukow P.O. Box 35, Protvino (Moscow Region), USSR
[38] Institute of Physics, University of Stockholm, Vanadisvägen 9, 11346 Stockholm, Sweden
[39] Dipartimento di Fisica Sperimentale, Università di Torino and INFN, Via P. Giuria 1, 10125 Turin, Italy
[40] Dipartimento di Fisica, Università di Trieste and INFN, Via A. Valerio 2, 34127 Trieste, Italy, and Istituto di Fisica, Università di Udine, 33100 Udine, Italy
[41] Department of Radiation Sciences, University of Uppsala, P.O. Box 535, 75121 Uppsala, Sweden
[42] Inst. de Fisica Corpuscular IFIC, Centro Mixto Univ. de Valencia-CSIC, and Departamento de Fisica Atomica Molecular y Nuclear, Univ. de Valencia, Avda. Dr. Moliner 50, 46100 Burjassot (Valencia), Spain
[43] Institut für Hochenergiephysik, Österreichische Akademie der Wissenschaften, Nikolsdorfergasse 18, 1050 Vienna, Austria
[44] Inst. Nuclear Studies and, University of Warsaw, Ul. Hoza 69, 00681 Warsaw, Poland
[45] Fachbereich Physik, University of Wuppertal, Postfach 100 127, W-5600 Wuppertal 1, Federal Republic of Germany

Received 16 October 1991

Abstract. The average lifetime of B hadrons produced in hadronic Z^0 decays has been measured with the DELPHI detector at LEP. The measurement is based on the analysis of the impact parameter distributions of high p_t muons and hadrons. The resulting mean B lifetimes are $\tau_B = (1.30 \pm 0.10 \pm 0.08)$ ps and $\tau_B = (1.27 \pm 0.04 \pm 0.12)$ ps respectively, giving a combined value of $\tau_B = (1.28 \pm 0.10)$ ps. The hadronic sample was also used to measure the partial Z^0 width $\Gamma_{b\bar{b}}/\Gamma_h$ and gave a value of $0.222 \,^{+0.033}_{-0.031} \pm 0.017$.

1 Introduction

In the context of the standard model, hadrons containing b quarks decay by flavor changing weak transitions in which the relative couplings of the quarks are described by the Cabibbo-Kobayashi-Maskawa mixing matrix. In the spectator model the lifetime of a B hadron is given by

$$\tau_B = \frac{192\pi^3}{G_F^2 m_b^5} \mathrm{Br_{sl}} (f_u |V_{ub}|^2 + f_c |V_{cb}|^2)^{-1} \quad (1)$$

where G_F is the Fermi constant, m_b is the b quark mass, $\mathrm{Br_{sl}}$ is the semileptonic branching ratio, and f_u and f_c are the products of a QCD correction term with phase space factors. Measuring the lifetime of B hadrons constrains the value of $|V_{ub}|$ and $|V_{cb}|$, once the branching ratio for semileptonic decays and the mass of the b quark are given.

The present work, using data from the DELPHI detector at LEP, extracts the average lifetime of B particles from the impact parameter distributions of two different charged particle samples. The first analysis uses muon candidates with high transverse momentum with respect to the jet axis and measures the average lifetime of the B hadrons produced in Z^0 decays weighted by their semileptonic branching ratios. It represents a standard technique and has an advantage in the high purity of the sample but the statistics are limited. The second approach, which is complementary, has not previously been used at LEP. It employs all tracks from hadronic events fulfilling the same kinematical cuts as used to define the muon sample, except for the muon identification criteria. This procedure takes advantage of the large B decay multiplicity and measures directly the average lifetime of all the B particles produced at the Z^0 resonance. The statistics are higher than in the muon sample but the signal to background ratio is lower. In consequence, higher tracking accuracy is needed in order to observe a clear signal from B decays in the shape of the impact parameter distribution.

There have been several measurements [1–6] of the average B lifetime at cm energies around 30–40 GeV. The characteristics of the LEP machine and the tracking performance of the DELPHI detector provide favourable conditions for this measurement. The production of B particles is enhanced at the Z^0 pole, relative to lower energies, and that of the charm background reduced. Also, the B particels have higher momenta. Consequently, the dependence of the mean impact parameter on the momentum spectrum of the parent B particles is weaker, so that systematic effects on the impact parameter connected with b quark fragmentation uncertainties play only a minor role. In addition, the smaller beam spot size at LEP and the track extrapolation resolution achieved with the DELPHI microvertex detector permit a clear lifetime signal to be seen, even with the second method which uses all the tracks.

2 The DELPHI detector

The DELPHI detector has been described in detail elsewhere [7]. Only the properties most relevant to this analysis are summarised here.

In the barrel region, the charged particle tracks are measured by a set of cylindrical tracking detectors whose axes are parallel to the 1.23 T solenoidal magnetic field and to the beam direction. The time projection chamber (TPC) is the main tracking device. It is a cylinder of 30 cm inner radius and 122 cm outer radius and a length of 2.7 m. For polar angles θ between 21° and 39° and between 141° and 159°, track reconstruction in the TPC is based on at least four space points. For polar angles between 39° and 141° up to 16 points can be used.

Additional precise $r\phi$ measurements, in the xy plane perpendicular to the magnetic field, are provided at larger and smaller radii by the outer and inner detectors. The outer detector (OD) has five layers of drift cells at radii between 198 and 206 cm and covers polar angles from 42° to 138°. The inner detector (ID) is a cylindrical drift chamber having inner radius of 12 cm and outer radius of 28 cm. It covers polar angles between 29° and 151°. It contains a jet chamber section providing 24 $r\phi$ coordinates surrounded by five layers of proportional chambers providing both $r\phi$ and longitudinal z coordinates.

The microvertex detector (VD) [8] used in this analysis was installed before the start of the 1990 run. It consists of two independent half-shells inserted between the beam pipe and the ID. Each half-shell contains two concentric layers of capacitatively coupled silicon microstrip detectors located at radii of 9 and 11 cm (see Fig. 1). They measure $r\phi$ coordinates over a length of 24 cm, and cover polar angles between 43° and 137°. The strip pitch is 25 μm and every second strip is read out by VLSI chips with serial analogue outputs. The measured intrinsic point resolution for single tracks is $\sigma_{\mathrm{intrinsic}} = 8$ μm. The high intrinsic resolution of the VD demands careful understanding of its internal alignment. Position monitoring systems, using lasers and capacitive sensors, showed that the microvertex detector structure and position were stable within a few μm throughout the whole period of data taking.

The relative positions of the microstrip detector modules were measured outside DELPHI both before and after the data-taking period to an accuracy of about 20 μm. Further alignment corrections were made using Z^0 events, especially $Z^0 \to \mu^+\mu^-$. These

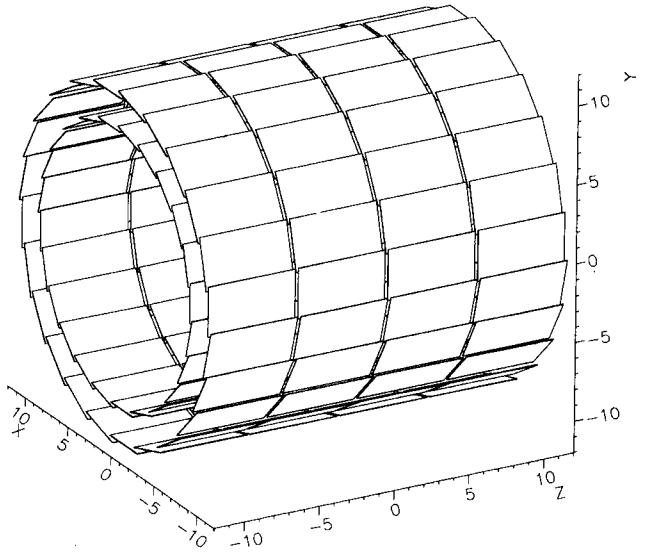

Fig. 1. Isometric view of the DELPHI Microvertex detector. The 24 cm long detector has two layers of silicon microstrip detectors at radii of 9 and 11 cm. Each layer is segmented azimuthally into 24 partially overlapping modules. Each module consists of two independent half-modules read out at the two ends of the detector. Each half-module is made of two daisy-chained detector plaquettes 5.8 cm long. In all there are 192 plaquettes and 54254 read-out channels. The whole detector is divided vertically into two structurally independent half-shells, located left and right of the beam pipe

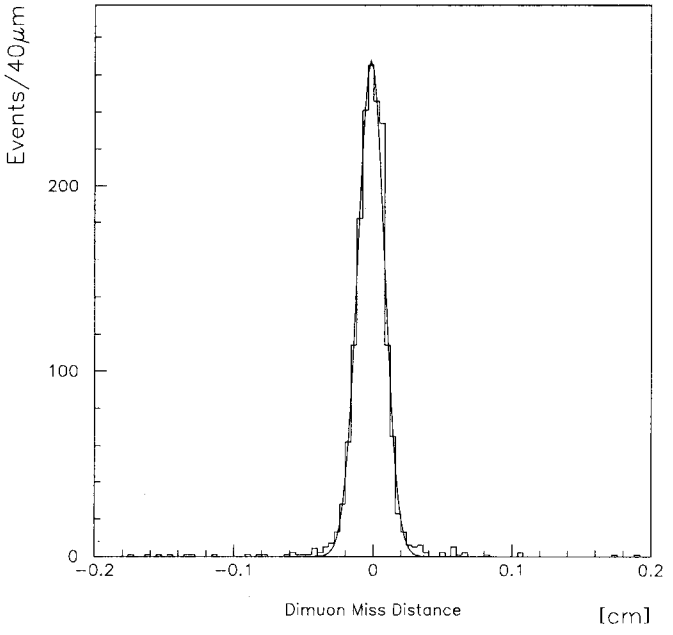

Fig. 2. The 'dimuon miss distance' distribution. This is defined as the apparent separation in the $r\phi$ plane of pairs of tracks in $Z^0 \to \mu^+\mu^-$ decays extrapolated to the interaction region. The fitted Gaussian has a width $\sigma = 95$ μm which corresponds to a track extrapolation accuracy of 67 μm

brought the alignment precision σ_{align} to about 8 μm and the final precision of individual $r\phi$ coordinate measurements in the VD, including alignment errors, to $\sigma_{\text{VD}} = (\sigma^2_{\text{intrinsic}} + \sigma^2_{\text{align}})^{\frac{1}{2}} = 11$ μm.

The extrapolation resolution at the vertex for high momentum tracks can be obtained from the width of the 'dimuon miss distance'. This is defined as the apparent separation in the $r\phi$ plane between pairs of tracks from $Z^0 \to \mu^+\mu^-$ decays extrapolated to the interaction region (see Fig. 2). The distribution is independent of the knowledge of the beamspot. The measured width of 95 μm implies an extrapolation resolution of 67 μm for 45 GeV/c particle tracks.

Muon identification in the barrel region is based on a set of muon chambers (MUB). The MUB covers polar angles between 53° and 127°. It consists of six active planes of drift chambers, two inside the return yoke of the magnet after 90 cm of iron (inner layer) and four outside after a further 20 cm of iron (outer and peripheral layers). The inner and outer layers have the same azimuthal coverage and the peripheral layer covers with a small overlap the dead spaces between them. Typically, therefore, a muon traverses either two inner layer chambers and two outer layer chambers, or just two peripheral layer chambers. Each chamber measures the $r\phi$ coordinate to ± 6 mm. Measuring $r\phi$ in both the inner layer and the outer or peripheral layer determines the azimuthal angle ϕ of muon candidates leaving the hadron calorimeter (HCAL) within about $\pm 1°$. These errors are much smaller than the effects of multiple scattering on muons traversing the calorimeters.

The background of misidentified hadrons in the selected muon sample was evaluated using the HCAL. This is a sampling gas detector incorporated in the magnet yoke. The calorimeter is divided into super-towers, each four layers deep, pointing at the interaction point. The energy resolution of the detector is $100\%/\sqrt{E}$.

3 Data analysis

3.1 Event selection

The present analysis is based on data collected by the DELPHI detector at LEP during 1990 at seven energies around the Z^0 pole. The integrated luminosity of 4.5 pb^{-1} provided about 120 000 hadronic events. The sample of hadronic events was selected by requiring

- at least 8 detected charged particles with momentum $p > 0.2$ GeV/c,
- a total energy detected in charged particles greater than 15 GeV, and
- a total energy detected in charged particles larger than 5 GeV in each of the two hemispheres with respect to the beam axis, i.e. $\cos\theta < 0$ and $\cos\theta > 0$.

Events were further required to have

- $|\cos(\theta^{\text{event}}_{\text{thrust}})|$ below 0.85, where $\theta^{\text{event}}_{\text{thrust}}$ is the polar angle of the thrust axis of the event,

- at least two tracks in each hemisphere, and
- the primary vertex reconstructed as described in Sect. 3.3.

Jets were reconstructed with the LUND algorithm LUCLUS with default parameters [9] using charged particles only.

Particles were used in the subsequent analysis only if belonging to a jet with

- thrust axis in the barrel region (defined by $|\cos\theta^{\text{jet}}_{\text{thrust}}| < 0.87$), and
- at least two charged particles with momentum above 2 GeV/c.

These cuts were to ensure that the direction of the thrust axis of the jet, defined as the axis maximising the sum of the absolute values of the projected longitudinal momenta of the charged particles in the jet, was adequately determined. When computing the p_t, the transverse momentum of a particle relative to the jet thrust axis, the jet thrust axis was redetermined after removal of this particle.

3.2 Impact parameter calculation

The impact parameter of a track is defined as its distance of closest approach to the Z^0 production point. Because of the much higher reconstruction accuracy in the $r\phi$ plane, only the projection of the impact parameter on this plane is used.

The projected impact parameter δ of a track from a particle with a proper decay time t is given by $\delta = \beta\gamma ct \sin\psi \sin\theta$, where θ is the polar angle of the parent particle and ψ the angle of the track with respect to the flight direction of the parent particle, projected in the $r\phi$ plane. For large values of $\beta\gamma$, this factor is on average cancelled by the decrease of the angle ψ, so that the ratio $\langle\delta\rangle/c\tau$, where τ is the average proper lifetime, becomes independent of $\beta\gamma$.

The jet thrust axis is used to estimate the direction of the decaying B particle. Thus the projected impact parameter is given a sign according to the position of the intersection of the track with the jet thrust axis (see Fig. 3). The sign is positive if the intersection point corresponds to a positive decay length.

Tracks reconstructed in the barrel tracking detectors were associated with hits in the VD as follows. First, in each layer, the VD hit closest to the extrapolation of the track was taken to be associated. The track was refitted including these hits. Any hit giving an excessive χ^2 contribution was rejected and the track again refitted without it. The track was then extrapolated to the interaction region.

For the impact parameter analysis, tracks were selected by requiring:

- momentum, p, above 3 GeV/c,
- momentum transverse to the jet axis, p_t, above 1 GeV/c, and
- two associated VD hits.

Asking for two VD hits to be included in the refitted track effectively eliminates wrong associations and gives the most precise extrapolation of the track to the vertex region. The kinematical cuts reduce multiple scattering effects, thus further improving the average track extrapolation accuracy, and also enhance the fraction of particles from b decay.

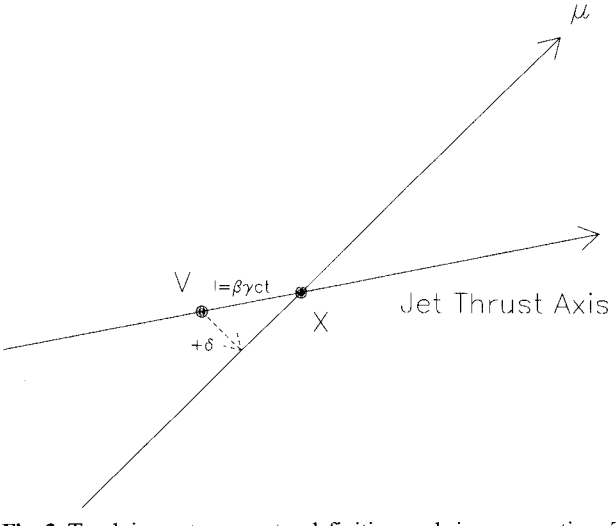

Fig. 3. Track impact parameter definition and sign convention. The B particle travels a distance $l = \beta\gamma ct$ along the flight direction approximately reproduced by the jet thrust axis. The impact parameter of decay product candidates is measured with respect to the reconstructed primary vertex V. The sign is given according to the point of intersection X, between the extrapolated track and the thrust axis of the jet. For the track in consideration, μ, the sign is positive. For a track crossing the thrust axis on the opposite side of the vertex the sign would be reversed

3.3 Primary vertex reconstruction

The impact parameter resolution is the convolution of the track extrapolation accuracy and the precision on the determination of the primary vertex position. Therefore the best possible knowledge of the primary vertex position is essential to obtain the optimal impact parameter resolution. At LEP the projection of the interaction region onto the $r\phi$ (xy) plane is elliptical with a Gaussian beam profile about 15 μm high (σ in y) and 200 μm wide (σ in x). Because of the high extrapolation accuracy given by the VD, the impact parameter resolution depends strongly on the azimuthal angle of the track, if just the average beam position is used to represent the Z^0 production point. Reconstructing the primary vertex for each individual event reduces this effect and thus improves the overall impact parameter resolution substantially.

A two step procedure was used for determining the primary vertex. First, primary vertices were reconstructed for all hadronic events. The primary vertex fit was based on the Kalman Filter algorithm [10]. This algorithm allows single tracks to be added or removed from the fit easily. Tracks were tested for compatibility with the primary vertex by calculating their individual χ^2 contribu-

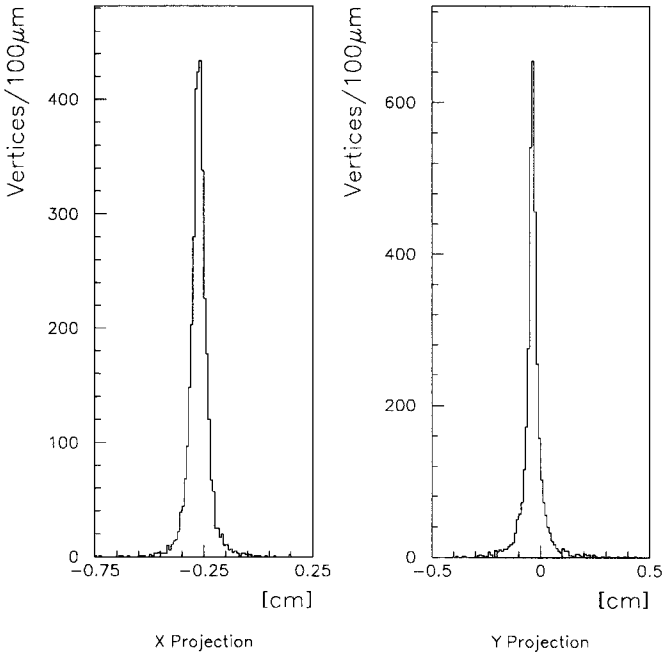

Fig. 4. Beam profile reconstructed in the horizontal (x) and vertical (y) coordinates for a single LEP fill. The different widths observed (the FWHM is 500 μm in x and 300 μm in y) reflect the different sizes of the LEP beam in the two planes. Since the beam position reconstruction does not include the beam constraint, the width in y indicates the reconstruction accuracy in the first step of the vertex fit procedure

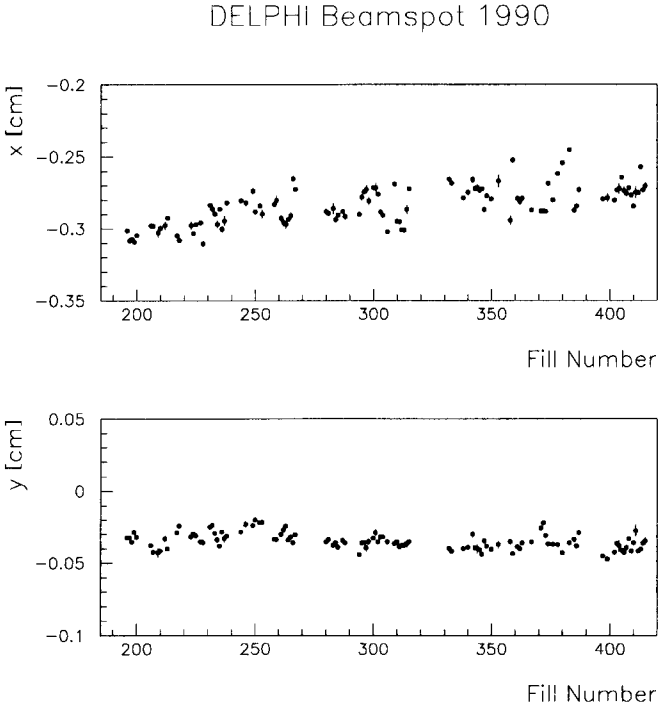

Fig. 5. Average beam position as a function of the LEP fill number, determined by reconstructing the event vertices. Only the larger error bars are visible

tions to the vertex fit. After scaling the track reconstruction errors appropriately the χ^2 probability distribution was flat, except for a peak at low probabilities. Such tracks, having a probability of less than 1%, were removed and the vertex refitted. Figure 4 shows the projected distribution of reconstructed vertices in one fill. The vertex reconstruction error depended on the number of tracks used in the vertex fit and on the event topology. It was typically ± 110 μm in the direction orthogonal to the event thrust axis.

These vertices were used to measure the average position and the width of the interaction region for each LEP fill (Fig. 5). Typically the mean beam position in a fill was reconstructed to better than 20 μm in both x and y.

Due to the small vetical size of the interaction region (≈ 15 μm), the reconstruction accuracy achieved in this first step can be deduced from the apparent vertical size. The horizontal size of the beam spot can then be determined by unfolding this reconstruction error from the apparent horizontal size. This was measured for all fills with sufficient statistics. No significant variation being observed from fill to fill, its means value, 200 μm, was used for the analysis.

As these mean beam positions were reconstructed using a large number of vertices, they are essentially independent of any individual event. Therefore, in a second step, an optimal estimate of each Z^0 production point was obtained by re-evaluating the vertex position including the beam constraint. The mean beam position in the fill was used to initialize the fit. Subsequently, tracks were tested for compatibility with this vertex position before being included in the final primary vertex estimate. After this procedure, the small vertical beam size dominates the y value but the fitted x value is more accurate than the average beam position. The impact parameter was therefore computed with respect to this fitted vertex. To avoid the bias due to the inclusion of the track in the fit, each track was removed from the vertex fit before computing its impact parameter.

This procedure was studied using the full detector simulation. For simulated b decays the tracks originating directly from the B hadron were identified and the reconstructed impact parameters studied. No evidence of a bias in the estimation of the impact parameter was found when computing the impact parameter with respect to the reconstructed primary vertex provided that, as in this analysis, the track itself was first excluded from the vertex fit.

Events were used in the following analysis only if four or more tracks contributed to the vertex fit and the mean beam position during the fill was determined with sufficient statistics.

3.4 Impact parameter resolution

The impact parameter resolution obtained when using the reconstructed primary vertex was studied as a function of the charged particle momentum component in the $r\phi$ plane. The resolution was estimated by fitting a Gaus-

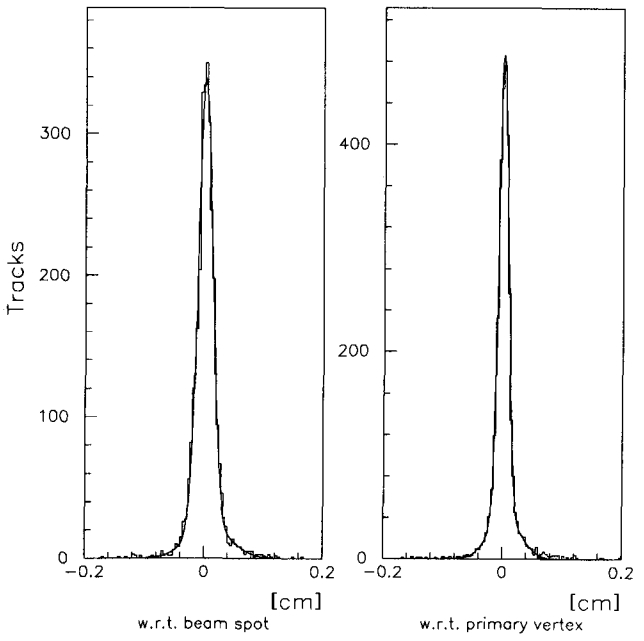

Fig. 6. Impact parameter distribution for hadronic tracks with a momentum component in the $r\phi$ plane, $p_{r\phi}$ larger than 10 GeV/c. The impact parameter is measured with respect to the average beam position in the fill (left) and the primary vertex of the event reconstructed using the beam constraint (right). The widths (σ) of the central Gaussians describing the resolution are 128 μm and 84 μm respectively

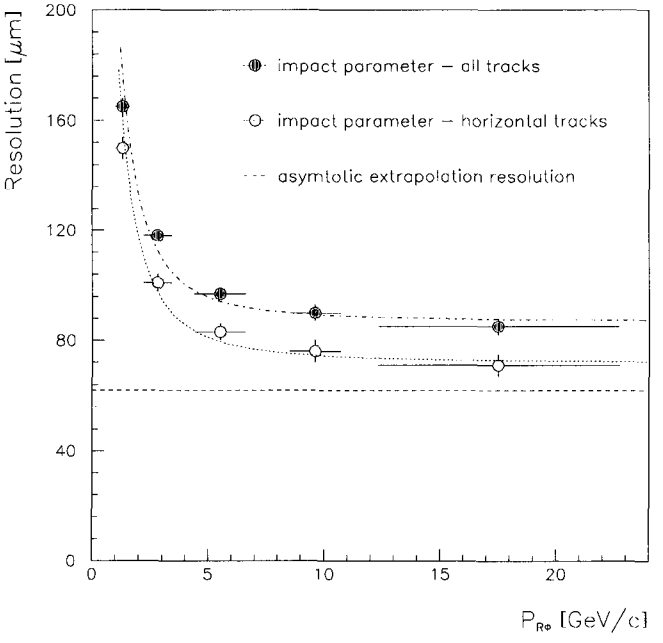

Fig. 7. Impact parameter resolution vs $p_{r\phi}$, the momentum component in the $r\phi$ plane, for hadron tracks linked with two VD hits. The values for the particles at less than 15° to the horizontal (open circles) are smaller as they have a reduced contribution from the width of the interaction region. The points are measurements. The curves represent the effect of the multiple scattering. The dotted line indicates the asymptotic track extrapolation accuracy

sian to the impact parameter distribution, ignoring the non-Gaussian tails extending outside two standard deviations. The resolution worsens for lower momenta due to the multiple scattering in the beam pipe and the inner VD silicon layer. Above 10 GeV/c, multiple scattering is negligible and the fitted width of the impact parameter distribution gives the intrinsic resolution. Using the primary vertex reconstructed event by event, this asymptotic value is 84 μm (Fig. 6 right). For comparison, the impact parameter distribution using the average beam position is also shown (Fig. 6 left).

As the height of the LEP beam spot is small, the effect of the error in the vertex position on the impact parameter is small for tracks at small angles to the horizontal plane. This allows the contributions to the impact parameter resolution from the track extrapolation error and the vertex reconstruction error to be distinguished. For high momentum tracks within $\pm 15°$ to the horizontal plane, the measured impact parameter resolution was 72 μm (see Fig. 7). Unfolding from this measured width the residual effect of the horizontal beam width and the error on the average beam position results in an estimate of 62 μm for the extrapolation accuracy for high momentum tracks. This compares well with the value of 67 μm extracted from the dimuon miss distance distribution as discussed in Sect. 2. These results imply an average resolution on the reconstruction of the event primary vertex of about $(84^2 - 62^2)^{\frac{1}{2}} = 57$ μm when including the beam constraint in the vertex fit.

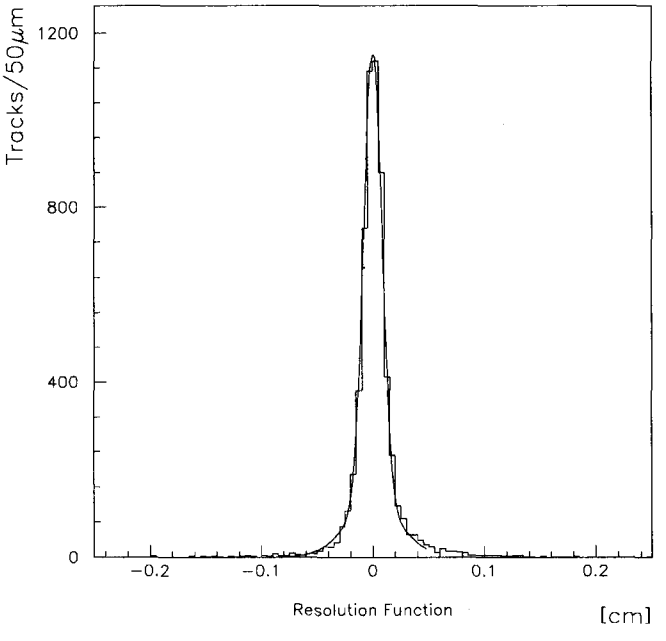

Fig. 8. Impact paramenter distribution for hadronic tracks with high p_t component along the z axis. The superimposed fitted curve is the sum of two Gaussians used to parametrize the resolution function. To reduce distortions due to residual lifetime effects, the tails on the positive side were excluded from the fit

The impact parameter resolution function, $R(\delta)$, used in the subsequent analysis, was determined from the data as follows. The tracks were selected with the same reconstruction quality and kinematical cuts as in the analyses. The subset of these tracks lying closest to the plane defined by the jet thrust direction and the z axis carry reduced lifetime information. They were therefore selected by requiring $|\sin \psi_{pt}| < 0.5$, where ψ_{pt} is the angle between the p_t vector and that plane. The impact parameter distribution of these tracks was then parametrized as the sum of two Gaussians (Fig. 8). Both were centred at zero. The resolution function was therefore represented by the sum of two Gaussians described by three parameters, σ_1 and σ_2 giving the two widths and f the fraction in the wider Gaussian. The narrower Gaussian had a width of 82 μm the wider one had a width of 245 μm and contained 22% of the tracks.

3.5 Muon identification and sample composition

Details of the identification procedure and of the analysis determining the sample composition are given in [11].

The extrapolated track positions were compared with the hits reconstructed in the MUB. The combination of hits giving the smallest χ^2 was chosen. Muon candidates were then selected by requiring the track to be linked to hits in two layers of the muon chambers, or at least in the peripheral layer, within 3 standard deviations of the track extrapolation both in the $r\phi$ coordinate and in the ϕ angle.

The efficiency of this selection was measured using dimuon events. To extrapolate this result to the case of lower energy muons produced inside jets, use was made of simulated data in which the chamber efficiencies and the rate of spurious hits were tuned to reproduce the real data. Four muons above 3 GeV/c, the efficiency ε_μ was found to be $(78.5 \pm 3.5)\%$, and to have no significant dependence on the energy of the muon or its momentum transverse to the jet axis.

The contamination from hadrons was measured from the real data. For high energy pions from $\tau \to 3\pi$ decay, the misidentification probability $\varepsilon_{\mu,\pi}$ was found to be $(1.1 \pm 0.3)\%$. At low energy, between 3 and 5 GeV/c, $\varepsilon_{\mu,\pi}$ was found to be below 1% for pions from $K_s^0 \to \pi^+\pi^-$ decay. Both these evaluations include the contributions of decays in flight but are limited by statistics.

To improve the precision, the energy deposit distributions of the candidates in the four layers of the HCAL were compared with those expected for hadrons of the same momentum, as predicted by the full detector simulation program, and with those observed for muons from $Z^0 \to \mu^+\mu^-$ decay. A correction was made for the overlaps between muons and hadrons expected inside jets. For particles with momentum between 10 and 15 GeV/c, this analysis gave $\varepsilon_{\mu,\pi} = (0.91 \pm 0.12 \pm 0.14)\%$, where the second error is the estimated systematic uncertainty. This does not include the contribution of decays in flight.

The final composition was evaluated by a χ^2 fit to the data of the 2-dimensional p and p_t spectra predicted by the Monte Carlo using the full detector simulation. The composition was then parametrised as a function of p_t, the momentum of the muon candidate transverse to the thrust axis of the rest of the jet, for muons having momenta above 3 GeV/c. The distribution of the transverse momentum for data and Monte Carlo agreed well over the whole p_t range. The integrated composition is given in Table 1 for the $p > 3$ GeV/c and $p_t > 1$ GeV/c cuts used in the analysis.

Table 1. Integrated sample composition for muon candidates with $p > 3$ GeV/c and $p_t > 1$ GeV/c

Muon source	[%]
Muons from direct b decays	50.0
Muons from cascade b decays	13.9
Muons from c decays	11.3
Muons from π, K decays	8.6
Hadronic contamination	16.1

4 *B* lifetime determination

4.1 High p_t muon sample

After applying the event and track selections and using the muon identification criteria described above, 839 muon candidates were found. Their impact parameter distribution showed a clear shift towards positive values, having a mean value of 151 ± 13 μm (Fig. 9). The b lifetime information was extracted from this distribution by an unbinned maximum likelihood fit.

The likelihood function used was the product of the inverse probability density functions

$$\mathscr{L}(\tau_B) = \prod_i P(\delta_i, \tau_B) \qquad (2)$$

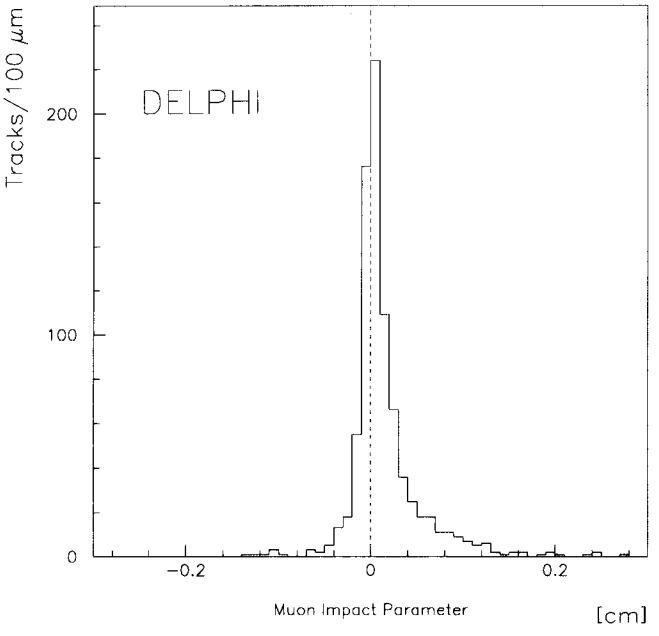

Fig. 9. Impact parameter distribution of high p_t muons. The mean impact parameter is 151 ± 13 μm

corresponding to the observation of a muon with a given value of impact parameter δ_i for the individual event.

For each track, i, the fitting function $P(\delta_i, \tau_B)$ was defined as the sum of the contributions from five sources:

- muons from direct $b \to \mu$ decays,
- muons from cascade $b \to c \to \mu$ decays and also, but less importantly, from $b \to \bar{c} \to \mu$ and $b \to \tau \to \mu$ decays,
- muons from $c \to \mu$ decays,
- muons from the decay of long lived hadrons (π, K),
- misidentified hadrons,

each weighted by the fraction of muons arising from that source:

$$P(\delta_i; \tau_B) = f_b(p_t) P_b(\delta_i; \tau_B) + f_{\text{casc}}(p_t) P_{\text{casc}}(\delta_i; \tau_B) + f_c(p_t) P_c(\delta_i) + f_{\text{dec}}(p_t) P_{\text{dec}}(\delta_i) + f_{\text{mis}}(p_t) P_{\text{mis}}(\delta_i). \quad (3)$$

The fractions $f_j(p_t)$, with $j = (b, \text{casc}, c, \text{dec}, \text{mis})$, are the probabilities that a muon candidate of given transverse momentum p_t came from each of these sources, as discussed in Sect. 3.5. The probability density functions P_j describe the impact parameter distributions for the various sources.

The probability density functions for muons from direct and cascade b decays and from c decays were evaluated in two steps.

Firstly the impact parameter distribution expected for a reference lifetime τ_0 was computed by Monte Carlo, disregarding tracking resolution effects. Hadronic events were generated using the Lund JETSET 7.2 parton shower model [9] with retuned parameters, the Peterson form of the longitudinal fragmentation function [12], and an improved description of b and c decays. Muons were required to pass the same p and p_t cuts as in the data. The impact parameter of each surviving muon track was evaluated using the exact trajectory and primary vertex position, as generated in the Monte Carlo, but its sign was determined using the reconstructed jet thrust axis. The distributions were then parametrized as the sum of four exponentials giving a corresponding "physics function" F_j, with $j = (b, \text{cas}, c)$. F_b is shown in Fig. 10. The distribution for any arbitrary lifetime τ was then found by scaling the reference distribution by the factor τ/τ_0. The F_{casc} function describing cascade b decays was scaled with only the b lifetime since the b lifetime dominates its shape. Possible distortions were avoided by choosing a reference lifetime τ_0 giving a scaling factor close to unity, namely $\tau_0 = 1.3$ ps. The charm physics function F_c was fitted to the impact parameter distribution of muons produced in simulated charm decays.

The second step was to convolute these scaled functions analytically with the experimental impact parameter resolution function $R(\delta)$ described in Sect. 3.4:

$$P_x(\delta; \tau_B) = \int F_x(\delta', \tau_B) R(\delta' - \delta) \, \mathrm{d}\delta' . \quad (4)$$

The background probability density function due to misidentified hadrons, P_{mis}, was determined from the data, using the tracks that satisfy the same selection criteria as the muon candidates except for the muon identification requirement.

The probability density function due to decays of long-lived hadrons, P_{dec}, was studied by Monte Carlo. The apparent impact parameter distributions of single decaying and non-decaying mesons from the primary vertex were simulated using the full DELPHI detector simulation. The tracks identified as muons were associated to VD hits and refitted, as in the real data. This allowed the effect of the kink at the decay to be studied. The use of the VD, at a small radius from the Z^0 production point, minimizes the effects of the decays in the detector. Both decaying and non-decaying hadrons contain some lifetime information from the b and c decays. To include this, a convolution function was found which gave the simulated non-decaying mesons the impact parameter distribution observed for the real hadrons. The simulated impact parameter distribution of the decaying mesons was then convoluted with this function to give the best estimate of their impact parameter distribution.

The result of the maximum likelihood fit was $\tau_B = (1.30 \pm 0.10)$ ps. Figure 11 shows the result of the fit, including the contributions from the different muon sources, superimposed on the data. The fitting procedure was tested using Monte Carlo data generated with different lifetimes. There was good agreement over the whole range of input lifetimes (1 to 1.8 ps).

The b lifetime was evaluated for various subsamples of the data, giving the results summarized in Table 2. The results obtained from muons of positive and negative charge agreed. Because of the good spatial resolution of the VD, the track extrapolation to the interaction region

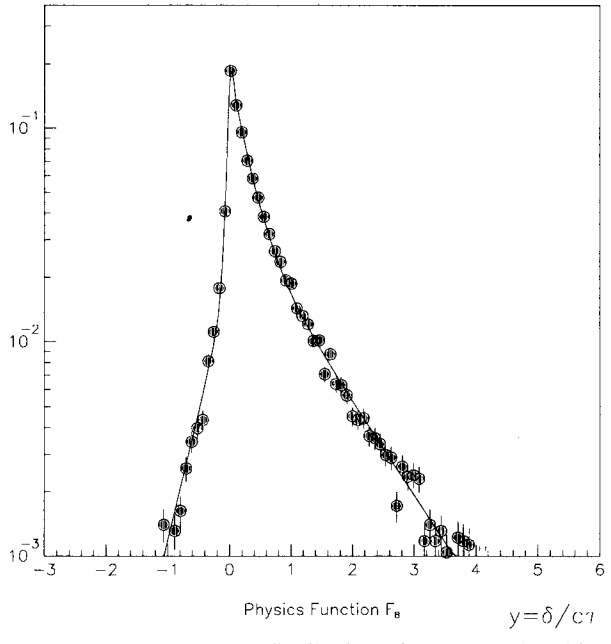

Fig. 10. Impact parameter distribution of muons produced in semileptonic b decays, predicted by the Monte Carlo, disregarding tracking resolution effects. The distribution has been normalized to 1. The corresponding physics function, F_b, is derived by fitting separately the positive and the negative side with two exponentials

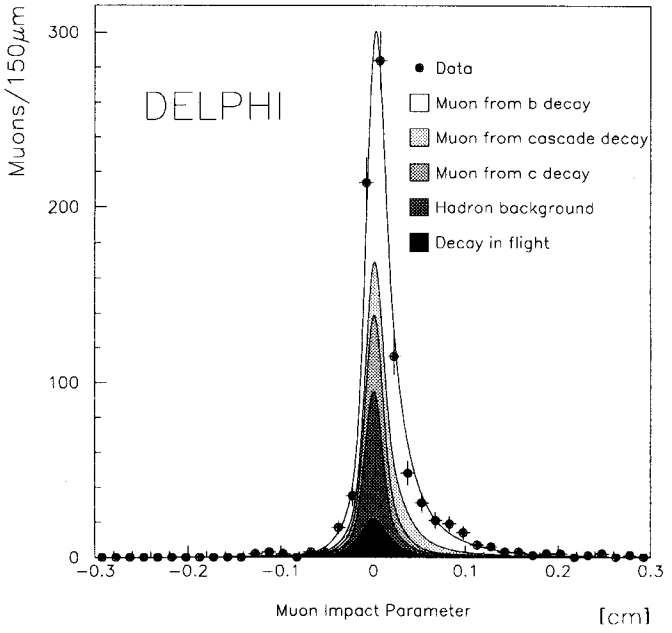

Fig. 11. Impact parameter distribution of high p_t muons with the fitted probability density functions, as derived from the likelihood fit, split into the five components considered in the fit. The result of the fit is $\tau_B = (1.30 \pm 0.10\,(\text{stat}))$ ps

Table 2. Summary of consistency checks on the muon sample

Selection	N_{tracks}	τ_B [ps]
Standard selection	839	1.30 ± 0.10
Positive charge tracks	439	1.28 ± 0.14
Negative charge tracks	400	1.32 ± 0.14
$\cos\phi > 0$	415	1.42 ± 0.15
$\cos\phi < 0$	424	1.19 ± 0.14
$\cos\theta > 0$	406	1.24 ± 0.14
$\cos\theta < 0$	433	1.35 ± 0.14
Mean beam position	839	1.35 ± 0.11

is determined mainly by the VD information. To check whether possible misalignments of a single VD half-shell affect the result, tracks measured in the two half-shells were separated by a cut in $\cos\phi$. The results agreed. Separating the tracks coming from positive and negative $\cos\theta$ also showed no systematic effect. To check for any possible bias arising from the use of a primary vertex position reconstructed individually for each event, the analysis was repeated using a fixed beam spot given by the average beam position measured for each fill. In this case it was necessary to reevaluate the resolution function to account for the degraded impact parameter resolution. This gives rise to a systematic uncertainty in the comparison. Within this uncertainty, the value obtained agreed with the previous result, as expected from the Monte Carlo study of Sect. 3.3.

The systematic errors for the final sample are summarized in Table 3. There are two main contributions. The first is due to the uncertain knowledge of the muon sample composition, the other to the uncertainties in parametrizing the physics functions and in evaluating the

Table 3. Systematic error evaluation for the muon sample

Source	Systematic error [ps]
Muon sample composition	0.05
Resolution function $R(\delta)$	0.04
Physics functions F_i	0.03
Decay background parametrization	0.03
Hadronic background parametrization	0.02
Average τ_C	0.02
Fragmentation effect on impact parameters	0.01
Total	0.08

impact parameter resolution. These errors are now discussed in turn.

The value ± 0.05 ps quoted as due to the error in the *composition of the high p_t muon sample* was evaluated by changing the various components within their errors, as derived from the fit to the muon spectrum. For the evaluation of the combined error, the correlations between the errors were taken into account. The error quoted also contains the effect of the uncertainty in b fragmentation and in the semileptonic branching fractions.

The effect of the uncertainty in the *parametrization of the impact parameter resolution function, $R(\delta)$*, was evaluated by varying the three parameters (σ_1 and σ_2 giving the two widths and f the fraction in the wider Gaussian) independently within their errors. To account for the correlation between the parameters, the full covariance matrix of the resolution function fit was used, giving a contribution of ± 0.04 ps.

The systematic errors coming from the *parametrizations of the physics functions, F_i*, were evaluated by varying their parameters by one standard deviation and accounting for correlations, as above. Summing in quadrature the estimated contributions from the F_b, F_{casc} and F_c functions gave an error of ± 0.03 ps.

For the contribution from the *decay background parametrization*, which relied on the Monte Carlo model, the effect of changing the K/π ratio and the momentum spectrum of decaying particles was also evaluated. Adding these contributions in quadrature with the effect of the uncertainty in the parametrization gave a value of ± 0.03 ps.

The systematic error in the *hadronic background parametrization* was obtained in the same way, by fitting the data and varying the parameters of the fitted functions according to their errors, giving ± 0.02 ps.

By varying the lifetimes of charmed mesons and baryons by one standard deviation, the systematic error due to the knowledge of the *average τ_C* was evaluated to be 0.02 ps.

As expected, the *b fragmentation* uncertainty had little effect on the predicted impact parameter distribution. Changing the ε_b parameter in the Peterson function to reproduce its uncertainty gave an effect of ± 0.01 ps. The effect on the high p_t muon sample composition was already accounted for.

Adding all these contributions in quadrature gave a total systematic error of ± 0.08 ps so that, in conclusion,

the result of the measurement using the muon sample was

$$\tau_B = (1.30 \pm 0.10 \pm 0.08)\ \text{ps}. \quad (5)$$

4.2 *High p_t hadron sample*

Charged hadrons were selected by applying the event and track selections given in Sect. 3.1, 3.2 and 3.3. The absolute value of the impact parameter was then required to be below 1.5 mm to reduce the contribution from decay products of long-lived particles. In addition, the track was required to be reconstructed in the OD as well as the TPC, and to have momentum below 25 GeV/c. These cuts selected 18 459 tracks. Their mean impact parameter was 40 ± 2 μm.

According to the Monte Carlo, 29% of the selected particles were from $Z^0 \to b\bar{b}$ events. As a check that the observed shift was due to a lifetime signal, particles belonging to the third or the fourth least energetic jet in a multijet event were separated out. In the jet ordering, only charged tracks were used. This sample is depleted in tracks carrying lifetime information because these least energetic jets are generally the gluon jets and therefore contain relatively few short lived particles. The mean impact parameter was found to be only 15 ± 6 μm, compared with 46 ± 2 μm for tracks in the two most energetic jets.

The b lifetime was extracted by comparing the impact parameter distribution of the whole sample with that of a corresponding Monte Carlo sample. For the latter, about 60 000 tracks fulfilling the same kinematical and geometrical acceptance cuts as the data were extracted from a set of hadronic events generated with the same JETSET 7.2 PS version with Peterson fragmentation as was used for determining the physics functions in the muon analysis. The resulting impact parameter distribution was convoluted with the measured impact parameter resolution. Then the Monte Carlo distribution was normalized to the data and the binned χ^2 was minimized with respect to the b lifetime. To avoid generating many distinct Monte Carlo data sets with different b lifetimes, a weighting technique was used. Monte Carlo events were produced assuming a reference lifetime τ_0. Then a weight $w(t, \tau_0, \tau_1)$ was attributed to each b decay track, where τ_1 is the desired lifetime and t the proper decay time of the b at the generation:

$$w(t, \tau_0, \tau_1) = \frac{\tau_0}{\tau_1} \exp\left(-t \frac{\tau_0 - \tau_1}{\tau_0 \tau_1}\right). \quad (6)$$

The fit procedure was tested on independent Monte Carlo samples generated with different values of τ_B. Good agreement was found over the whole range of input lifetimes.

The result of the fit was $\tau_B = (1.27 \pm 0.04)$ ps, assuming the value of $\Gamma_{b\bar{b}}/\Gamma_h = 0.217$ for Z^0 decay, as given by the standard model. The fit had $\chi^2/\text{n.d.f.} = 1.30$. Figure 12 compares the observed impact parameter distribution with the Monte Carlo prediction for the fitted b lifetime.

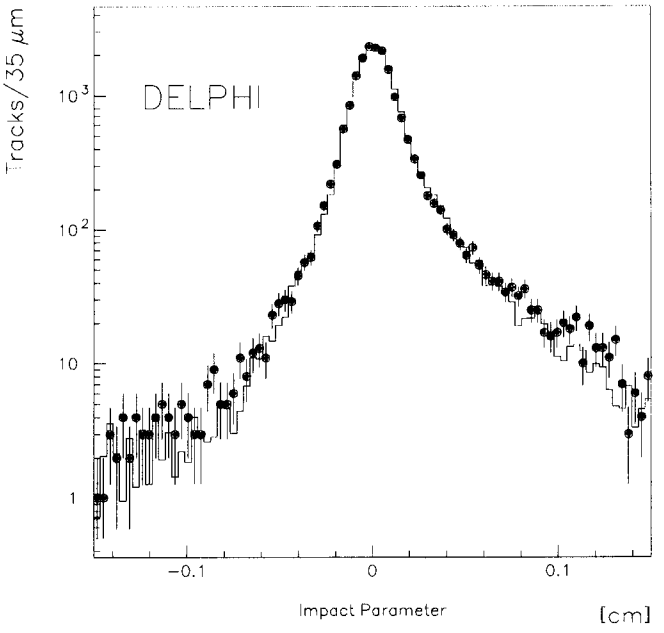

Fig. 12. Impact parameter distribution of hadronic tracks in the selected hadron sample. The points represent the data. The solid histogram shows the Monte Carlo simulation giving the best fit and corresponding to $\tau_B = 1.27$ ps

Several subsamples were selected for studying possible systematic biases. In particular, the mean value of the impact parameter distribution was studied as a function of θ and ϕ to search for indications of local misalignments or misalignments between the two VD half-shells. No such effects were found. Also, the minimum number of entries in each bin used in the χ^2 computation, which had been set to five, was varied, as was the number of histogram bins. The cut on the absolute value of the impact parameter was moved from 1.5 mm to 2.5 mm. All these checks gave no indication of any systematic bias. The total hadronic track sample was then sub-divided into different subsamples for which the lifetime was determined separately, as for the muon sample, and the analysis was repeated using the average beam position in the fill for the Z^0 production point. All the results obtained were consistent, as can be seen in Table 4.

The systematic errors connected with the measured impact parameter resolution function and with the Monte Carlo model are summarised in Table 5. They were evaluated as follows.

Table 4. Summary of consistency checks for the hadron sample

Selection	N_{tracks}	τ_B [ps]
Standard selection	18 459	1.27 ± 0.04
Positive charge tracks	9 144	1.32 ± 0.06
Negative charge tracks	9 315	1.23 ± 0.06
$\cos\phi > 0$	9 607	1.29 ± 0.06
$\cos\phi < 0$	8 852	1.24 ± 0.06
$\cos\theta > 0$	9 359	1.31 ± 0.06
$\cos\theta < 0$	9 100	1.22 ± 0.06
Mean beam position	18 459	1.29 ± 0.06

Table 5. Summary of systematic errors in the hadron sample analysis

Source	Systematic error [ps]
Resolution function	0.08
b fragmentation, ε_b	0.05
Transverse momentum distribution σ_q	0.04
Mean charged multiplicity in B decay	0.03
B baryon production	0.02
C baryon production	0.01
c fragmentation, ε_c	0.01
c lifetimes	0.03
Thrust axis uncertainty	0.03
Total	0.12

The first source of systematic error is associated to the uncertainty of *parametrization of the impact parameter resolution function.* The procedure used was the same as for the muon sample. The error is larger than for the muon sample because a much smaller proportion of the tracks carry lifetime information.

The second set of systematic errors is connected with the Monte Carlo generation, since the predicted composition of this sample involves several parameters optimized to fit the available data on general event variables at the Z^0 pole.

The *Peterson fragmentation function parameter* ε_b was tuned to reproduce the average of the values measured by DELPHI [11] and the other experiments at LEP [13–15] of the mean fraction of the beam energy taken by B hadrons, $\langle x_E \rangle_b = 0.695 \pm 0.012$, and varied to reproduce its uncertainty. A further check was made by changing the form of the longitudinal fragmentation function. The LUND symmetric function modified according to the Bowler space-time picutre of string evolution [16] implemented in JETSET 7.3 was used. It reproduced the measured $\langle x_E \rangle_b$ value within the errors but its shape differed from that of the Peterson function. The resulting lifetime agreed with that obtained with the Peterson scheme. On the basis of these checks, the overall systematic error due to the b fragmentation uncertainty was estimated to be ± 0.05 ps.

The width of the *transverse momentum distribution* of primary hadrons, σ_q, initially set to 0.37 GeV/c, was varied by ± 0.03 GeV/c and from the change of the fitted lifetime a contribution of ± 0.04 ps was evaluated.

The proper tuning of the above parameters ε_b and σ_q could be verified within this analysis. Since they affect the p and p_t spectra of b and primary particles, a systematic change of the measured lifetime as the p and p_t cuts are varied would indicate an incorrect value of ε_b or σ_q. Using the central values, the value of τ_B indeed remained constant within 2% when the momentum cut was changed between 3.0 and 9.0 GeV/c and within 5% when the transverse momentum cut was varied between 0.8 and 2.0 GeV/c. The variations were not systematic and were fully consistent with being due to statistical fluctuations. However, changing ε_b or σ_q outside the above ranges introduced a systematic correlation between the values of the kinematical cuts and the fitted lifetime.

The *mean charged decay multiplicity in B decay* was varied according to the uncertainty of the CLEO measurement of 5.5 ± 0.2 [17], giving an error of ± 0.03 ps.

As there is a large uncertainty in the *production of B baryons* at the Z^0 pole, the fraction of b decay into baryons was changed from the Monte Carlo prediction of 9.6% in the range of 5% to 20%. The corresponding systematic error contribution was ± 0.02 ps.

To account for uncertainties in *C baryon production* its contribution was also changed by a factor two, reproducing the discrepancy between the predictions of the JETSET and HERWIG [18] generators. This gave an additional error of ± 0.01 ps.

At present, knowledge of *charm fragmentation* at LEP energy is poorer than that of b fragmentation and relies on the measurements in [13, 14]. Combining these with an extrapolation to LEP energy from previous measurements of PEP and PETRA [19, 20] gives $\langle x_E \rangle_c = 0.52 \pm 0.03$. However, this uncertainty contributed a systematic error of only ± 0.01 ps.

Adding in quadrature all these contributions gave a systematic error from the uncertainty in the composition of the high p_t hadron sample of ± 0.07 ps.

In the Monte Carlo simulation, the *lifetimes of all charmed mesons* were set to their world average values [21] and charmed baryons were attributed the same lifetime as the Λ_c. All the charm lifetimes were then increased and decreased by one standard deviation. The result indicated a systematic error of ± 0.03 ps due to the uncertainty in the charm lifetimes.

An additional source of systematic errors in the Monte Carlo model is connected with the *reconstruction of the jet thrust axis.* In order to check its influence on the lifetime measurement, data and Monte Carlo variables sensitive to the thrust axis reconstruction were studied. Firstly the difference in azimuthal angle between the selected particles and the jet thrust was computed. Comparing data with the Monte Carlo distribution gave a χ^2 value of 135 for 100 bins, showing a reasonable agreement. To study any effect, an extra thrust axis smearing was then added to the Monte Carlo. Smearing values exceeding 15 mrad significantly increased the value of χ^2 for this comparison. This value is 25% of the average angle between the parent B particle and the reconstructed jet thrust axis. The lifetime was evaluated with a Monte Carlo sample including such an additional 15 mrad thrust axis smearing. As a second check the lifetime was evaluated using only particles whose azimuthal angle was more than 50 mrad from the jet thrust axis. These particles are less affected by thrust reconstruction errors and by any possible differences between data and Monte Carlo. From these checks a systematic uncertainty of 0.03 ps was assigned.

Adding all these contributions in quadrature resulted in a total systematic error of ± 0.12 ps. In conclusion, therefore, the result of the measurement using the hadronic track sample was

$$\tau_B = (1.27 \pm 0.04 \pm 0.12)\ \text{ps}. \quad (7)$$

5 Results and discussion

In summary, the average b hadron lifetime τ_B was found to be $(1.30 \pm 0.10 \pm 0.08)$ ps from the analysis of the high p_t muon sample and $(1.27 \pm 0.04 \pm 0.12)$ ps from the analysis of the hadron sample, where the first error is statistical, the second systematic.

The average lifetime from the muon sample is weighted by the semi-leptonic branching ratios, which are proportional to the lifetimes, while the lifetime measured from the hadron sample is weighted by the mean charged multiplicity of the different B species. If then the lifetimes of different B particles produced in Z^0 decays differ significantly, the value measured from the two samples should also differ. Assuming equal production of two dominant B species, as of charged and neutral B mesons, with different lifetimes, $\tau^{\pm}$ and τ^0, the ratio of the two average values can be predicted as a function of the ratio of the lifetimes. This prediction can then be compared with the observed ratio. However, the present data only constrain the ratio between $\tau^{\pm}$ and τ^0 to be below 3 at 68% confidence level. For comparison, processes outside the spectator model are expected to lead to a lifetime difference between various B particles of no more than about 10% [22]. In the following, it was therefore assumed that the two lifetimes are equal.

The two lifetime measurements can be combined using a weighted least squares procedure. As the systematic errors are only partially decoupled, the correlations must be taken into account. This was done by constructing a correlation matrix $\rho_{i,j}$ between the various error sources in the two measurements. The covariance of the measurements is then given by $\mathrm{cov}(\tau_\mu, \tau_h) = \sum_{i,j} \rho_{ij} \sigma_{\mu,i} \sigma_{h,j}$. The systematic errors were grouped as shown in Table 6. The correlated errors are those from common sources, namely the uncertainties in fragmentation, in τ_c and in the experimental resolution. The correlation coefficient ρ for these errors was conservatively assumed to be maximal (i.e. $\rho = 1$). For all other errors $\rho = 0$ was taken. Due to the overlap between the two event samples, the statistical errors of the two measurements are also partially correlated. This was taken into account by evaluating a correlation coefficient $\rho = 0.3$ for the statistical errors. The combined lifetime was then derived by the least squares estimate giving

$$\tau_B = (1.28 \pm 0.10)\ \mathrm{ps}. \tag{8}$$

This value agrees well with previous measurements at lower cm energies and also with a recent measurement at LEP [23]* (see Table 7).

This lifetime measurement can be used to constrain the Cabibbo-Kobayashi-Maskawa matrix element $|V_{cb}|$ (see (1)). The ratio $|V_{ub}|/|V_{cb}|$ has been determined to be 0.1 to 0.2 in a model dependent way [5]. The semileptonic branching ratio $\mathrm{Br}_{sl} = (10.4 \pm 0.6 \pm 0.5)\%$ has been derived using DELPHI data [11]. The phase space and QCD correction terms f_u and f_c have been evaluated following [22] but imposing the quark mass difference value $m_b - m_c = (3.30 \pm 0.02)\ \mathrm{GeV/c^2}$ [27], which was obtained by fitting the lepton spectrum in semileptonic B decays, and using $\alpha_s(m_b^2) = 0.20 \pm 0.02$, which has been obtained by extrapolation from the newly measured DELPHI value of $\alpha_s(m_Z^2) = 0.113^{+0.007}_{-0.006}$ [28]. Neglecting $|V_{ub}|$ then gives

$$|V_{cb}| = (0.045 \pm 0.002 \pm 0.002) \cdot (4.95/m_b) \tag{9}$$

where the first error is associated to this measurement of τ_B, the second to the uncertainties in $m_b - m_c$, in the QCD

Table 6. The systematic errors (in ps) correlated between the two anlyses grouped according to their common sources, together with the statistical error and other uncorrelated systematic errors

	Error source	ρ	Muon sample	Hadron sample
Correlated	Resolution	1	0.04	0.08
	Fragmentation	1	0.02	0.05
	c lifetime	1	0.02	0.03
	Statistical	0.3	0.10	0.04
Uncorrelated	Systematic	0	0.07	0.06

* Since the completion of this paper, a measurement [24] of the B lifetime of (1.32 ± 0.12) ps using high transverse momentum leptons at LEP has been published by the L3 collaboration

Table 7. Summary of measurements of τ_B using hadrons at lower energies or using high p_t leptons. These measurements do not depend on the value of $\Gamma_{b\bar{b}}$. Systematic and statistical errors are added quadratically

Experiment	E_{cm} [GeV]	Sample	τ_B [ps]	References
HRS	29	leptons	$1.02^{+0.42}_{-0.39}$	[1]
MAC	29	hadrons	1.29 ± 0.33	[2]
DELCO	29	leptons	$1.17^{+0.32}_{-0.27}$	[3]
MARK II	29	leptons	0.98 ± 0.18	[4]
TASSO	35	hadrons	1.35 ± 0.26	[5]
JADE	35	hadrons	$1.36^{+0.25}_{-0.23}$	[6]
ALEPH	91	leptons	1.29 ± 0.12	[23]
DELPHI	91	leptons only	1.30 ± 0.13	this expt.
World average			1.24 ± 0.07	

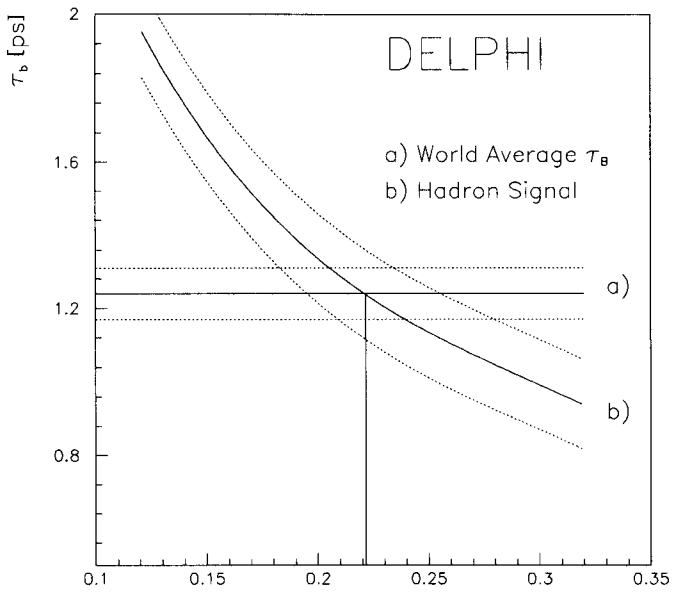

Fig. 13. Variation of the b lifetime measured from the hadron sample vs $\Gamma_{b\bar{b}}/\Gamma_h$. The curves show the computed dependence with one standard deviation errors. The horizontal lines represent the world average of τ_B values that are independent of $\Gamma_{b\bar{b}}/\Gamma_h$, as given in Table 7. The vertical line indicates the measurement of $\Gamma_{b\bar{b}}/\Gamma_h$

correction factor, and (most importantly) in the semileptonic branching ratio. The dependence on the value assumed for m_b (in GeV/c^2) is displayed explicitly. The value of $|V_{cb}|$ is reduced by 0.001 by assuming the ratio $|V_{ub}|/|V_{cb}| = 0.15$.

The measurements of the b lifetime with high p_t lepton samples in this and in orther experiments and with hadron samples at lower energies are summarized in Table 7. These values do not depend on the partial decay width $\Gamma_{b\bar{b}}$ at the Z^0 pole. On the other hand the value from the hadron sample obtained in the present analysis depends strongly on the standard model value for $\Gamma_{b\bar{b}}$. Therefore $\Gamma_{b\bar{b}}$ can be constrained by comparing the value obtained from the hadron sample with the other values. To do this, the lifetime τ_B was evaluated from the hadron sample assuming a series of different $\Gamma_{b\bar{b}}/\Gamma_h$ values. The result is shown in Fig. 13, where the apparent b lifetime varies inversely with the assumed Z^0 branching ratio to b quarks. Using the world average value of τ_B derived from Table 7, namely $\tau_B = (1.24 \pm 0.07)$ ps, gave

$$\Gamma_{b\bar{b}}/\Gamma_h = 0.222 \begin{matrix} +0.033 \\ -0.031 \end{matrix} \pm 0.017 \qquad (10)$$

where the first error is due to the combined statistical and systematical errors on the present measurement using the hadron sample and the second error is that due to the uncertainty in the computed average of the b lifetime. Using $\Gamma_h = 1.726 \pm 0.016 \pm 0.011$ GeV, as measured by DELPHI [26], this gives

$$\Gamma_{b\bar{b}} = \left(383 \begin{matrix} +64 \\ -60 \end{matrix}\right) \text{MeV} \qquad (11)$$

in good agreement with the standard model prediction.

Acknowledgements. We are greatly indebted to our technical collaborators and to the funding agencies for their support in building and operating the DELPHI detector, and to the members of the CERN-SL division for the superb performance of the LEP collider.

References

1. J.M. Brown et al., HSR Coll.: Phys. Lett. 195B (1987) 301
2. W.W. Ash et al., MAC Coll.: Phys. Rev. Lett. 58 (1987) 640
3. D.A Klem et al., DELCO Coll.: Phys. Rev. 37D (1988) 41
4. R.A. Ong et al., MARK II Coll.: Phys. Rev. Lett. 62 (1989) 1236
5. W. Braunschweig et al., TASSO Coll.: Z. Phys. C - Particles and Fields 44 (1989) 1
6. J. Hagemann et al., JADE Coll.: Z. Phys. C - Particles and Fields 48 (1990) 401
7. P. Aarnio et al., DELPHI Coll.: Nucl. Instrum. Methods A303 (1991) 233
8. V. Chabaud et al.: Nucl. Instrum. Methods A292 (1990) 75
9. T. Sjöstrand, M. Bengtsson: Compt. Phys. Commun. 43 (1987) 367
10. P. Billoir, R. Frühwirt, M. Regler: Nucl. Instrum. Methods A241 (1985) 115
11. P. Aarnio et al., DELPHI Coll.: Partial width of the Z^0 into $b\bar{b}$ final states and mean b semileptonic branching fraction, Delphi Note 91-49 Phys 104, submitted to Geneva LP-HEP '91 Conference
12. C. Peterson et al.: Phys. Rev. 27D (1983) 105
13. D. Decamp et al., ALEPH Coll.: Phys. Lett. 244B (1990) 551
14. M.Z. Akrawy et al., OPAL Coll.: Phys. Lett. 263B (1991) 311
15. B. Adeva et al., L3 Coll.: Phys. Lett. 261B (1991) 177
16. M.G. Bowler: Z. Phys. C - Particles and Fields 11 (1981) 169
17. B. Gittelman, S. Stone: CLNS-87/81 (1987)
18. G. Marchesini, B.R. Webber: Nucl. Phys. B310 (1988) 461
19. J. Chrin: Z. Phys. C - Particles and Fields 36 (1987) 163
20. T. Sjöstrand, in: Z. Physics at LEP 1, CERN 89-08 (1989), Vol. 3, p. 310
21. Particle Data Group: Phys. Lett. 239B (1990)
22. J.H. Kühn et al., in: Z. Physics at LEP 1, CERN 89-08 (1989), Vol. 1, p. 267
23. D. Decamp et al., ALEPH Coll.: Phys. Lett. 257B (1991) 492
24. B. Adeva et al., L3 Coll.: Phys. Lett. 270B (1991) 111
25. H. Albrecht et al., ARGUS Coll.: Phys. Lett. 254B (1990) 409
R. Fulton et al., CLEO Coll.: Phys. Rev. Lett. 64 (1990) 16
26. P. Abreu et al., DELPHI Coll.: Nucl. Phys. B367 (1991)
27. H. Albrecht et al., ARGUS Coll.: Phys. Lett. 249B (1990) 359
28. P. Abreu et al., DELPHI Coll.: CERN-PPE/91-181, submitted to Z. Phys. C - Particles and Fields